Hindawi
Advances in Materials Science and Engineering
Volume 2019, Article ID 3409561, 14 pages
https://doi.org/10.1155/2019/3409561

Research Article

H-M Bearing Capacity of Cone-Shaped Foundation for Onshore Wind Turbine under Monotonic Horizontal Loading

GuoQi Xing, ChangJiang Liu, ShanShan Li, and Wei Xuan

College of Civil Engineering and Architecture, Weifang University, Weifang, China

Correspondence should be addressed to ChangJiang Liu; btlcj@163.com

Received 10 July 2019; Revised 11 October 2019; Accepted 28 October 2019; Published 17 December 2019

Academic Editor: Tomasz Trzepieciński

In this paper, monotonic horizontal loading tests were carried out to study the bearing capacity of the cone-shaped foundation in marine fine sand. With load-controlled methods, the horizontal load was applied to the rod of cone-shaped foundation at loading eccentricity ratios of 5.0, 6.0, and 7.0. In addition, theoretical analysis was used to investigate the horizontal ultimate bearing capacity, and finite element analysis was also used in this paper to investigate the influence factors of the bearing capacity of cone-shaped foundation. Based on the theoretical analysis, the formula for horizontal ultimate bearing capacity was deduced. Test results show that, at the same loading eccentricity, cone-shaped foundation can provide higher *H-M* bearing capacity as well as lower lateral deflection compared to regular circular foundation for wind turbines. In addition, the deflection-hardening behavior of load-deflection curve for cone-shaped foundation is also observed. Numerical analysis results show that the *H-M* bearing capacity of the cone-shaped foundation increases with increasing aspect ratio and buried depth, however, and decreases with increasing loading eccentricity. Based on the results from finite element analyses, several equations to calculate the maximum moment bearing capacities are put forward, which take the aspect ratio, loading eccentricity, and embedded depth into account.

1. Introduction

Due to energy shortage, environmental pollution, and greenhouse effect in the world, clean energy and renewable energy were widely exploited and utilized nowadays [1]. Wind energy resources were part of clean energy, which had the advantage of pollution-free and wide distribution. Wind power generation is a way of utilizing wind resources, which can be divided into offshore wind power and onshore wind power [2]. Compared to offshore wind power, convenience installation and low cost in maintenance works for onshore wind power made it to be widely used on the mainland, especially in the mountain area [3]. The bearing capacity and deformation for the foundation of onshore wind power subjected to the combined action of vertical loading, horizontal loading, and moment loading should be satisfied, which can make the onshore wind power work well [4].

For the foundation of onshore wind turbines, the method of model test is often used. Wakile [5] investigated the horizontal bearing capacity of foundation in sandy soil. A formula for horizontal bearing capacity of foundation in dense sandy soil was obtained, and the effect of compactness for sandy soil and dimension of foundation on horizontal bearing capacity was also studied by Govoni et al. [6, 7].

In addition, the numerical simulation method was also used in analysis. Ibsen et al. [8] put forward a theoretical formula for horizontal bearing capacity of foundation, considering the internal friction angle for sandy soil. Garakani and Ghaffar [9] studied the effect of embedment depth of foundation and internal friction angle for soil on bearing capacity of foundation subjected to static loading, and a formula for bearing capacity of foundation was put forward, which was also verified. Shrestha and Ravichandran [10] put forward an evaluation method of stability for foundation according to investigating the effect of distribution of earth pressure for soil around foundation subjected to horizontal loading and stiffness change of foundation and parameters for soil under foundation on bearing capacity. Biswas and Krishna [11] studied the effect of parameters for soil on horizontal bearing capacity of foundation embedded in nonhomogeneous soil. Based on practical projects, Mohamed and Austrell [12] analysed the effect of vertical loading and parameters for soil on horizontal bearing capacity and deformation for deep-buried foundation and shallow-buried foundation.

Besides, some other scholars studied the foundation with the combination method of theoretical analysis and numerical simulation. Meyerhof [13] studied the bearing capacity of spudcan foundation in homogeneous soil. Liu et al. [14] investigated the interaction between foundation and soil. Based on the limit analysis method, Luan et al. [15] obtained the lateral bearing capacity and the failure mechanism for multibucket foundation. In addition, using the method of three-dimensional finite element numerical analyses, Fan and Gao [16] investigated the lateral bearing capacity of pile foundations for cross-sea bridge.

In this paper, based on the spudcan foundation [17], a new type foundation for the onshore wind turbine was proposed, which was called cone-shaped foundation (CSF), as shown in Figure 1. For the cone-shaped foundation, mainly used in mountainous areas, gravels produced during excavation can be the part of the foundation. For the isolation layer with flexible rubber in cone-shaped foundation, it can reduce bending moment acting on the foundation and the stability of superstructure can be guaranteed. More importantly, gravels produced during excavation were fully utilized, which had an impact on the environment around cone-shaped foundation. The cone-shaped foundation had been successfully applied for patent in China [18]. This paper focused on the bearing capacity of cone-shaped foundation subjected to static loading compared to conventional circular foundation for the onshore wind turbine. In addition, the factors which affected the bearing capacity were also studied based on the numerical simulation method.

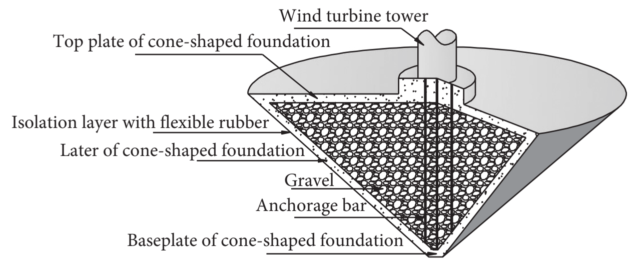

Figure 1: Cone-shaped foundation.

2. Test Model and Testing System

2.1. Test Model. In order to investigate the bearing capacity for cone-shaped foundation, the model test should be carried out in laboratory. Therefore, based on the dimension of full-scale foundation for the onshore wind turbine [19], the scale model for regular circular foundation (CF) was made with steel, which weight was 242.6 N, as shown in Figure 2(a). On the basis of the principle of equal volume, the scale model for cone-shaped foundations was also made with steel, as shown in Figure 2(b). The dimension in detail for the two foundation is shown in Figures 3(a) and 3(b). Moreover, the loading setup is shown in Figure 4(a), and the sign convention of displacement and load for plane loading of cone-shaped foundation is shown in Figure 4(b). In addition, the loading rod (15 mm in diameter) can be embedded in the top of foundation, with a density of 78 kN/m^3 and 1000 mm in length. The reference point for circular foundation and cone-shaped foundation was on the center of the top of foundation, as shown in Figure 4(b).

2.2. Tank. In this study, all tests were carried out in a tank with dimensions of 1.2 m × 1.2 m in plan and a height of 1.0 m (Figure 5). For the dimensions of the tank used in the test, they were considered big enough to eliminate the boundary effects. In order to prevent the lateral deformation of four sidewalls of the tank, square steels were used to strength the four sidewalls. In addition, in order to control the water level and drain the water out of the tank, a drain valve was installed at the bottom of the tank.

2.3. Displacement Sensor for Testing. In Figures 5(a) and 5(b), the linear variable differential transformer (LVDT) was mounted horizontally touching the loading rod to measure the corresponding horizontal deflection. In addition, as shown in Figure 5(b), the interval between LVDT1 and LVDT2 was 300 mm and the distance from LVDT2 to the top of the foundation was 350 mm. The measurement range for LVDT1 and LVDT2 was 0~50 mm, and the accuracy was 0.0125 mm. Besides, the inclination rate of the foundation model can be determined based on the recorded horizontal displacement of LVDT1 and LVDT2 and the interval between LVDT1 and LVDT2 [20]. Moreover, the horizontal displacement measured by LVDT1 and the corresponding applied horizontal load were utilized to determine the loading-deflection curve. In order to obtain outputs of all LVDTs automatically, a data acquisition system was used in test, as shown in Figure 5(a).

2.4. Sand Used in Test. The natural fine sand used for the tests was collected from Bohai Bay Beach in Weifang, East China. The particle size distribution curve for the fine sand is plotted in Figure 6. Physical parameters of the sand are shown in Table 1, all obtained from laboratory tests. As can be seen from Table 1, the soil belonged to homogeneous fine sand.

2.5. Preparation of Saturated Sand. During the test, in order to make water level drop uniformly during drainage by opening the valve at the bottom of the tank, gravels should be first scattered uniformly to a thickness of 6 cm, which had the particle size range of 16~22 mm, as shown in Figure 5(b). Moreover, a sheet of geotextile was covered on the surface of scattered gravels to prevent natural fine sand from being washed away during drainage. In order to obtain the saturated fine sand, enough water was poured into the tank. In order to ensure the homogeneity of sand formation, the dry marine fine sand should be sprayed into the tank. When the sand bed had reached a height of 55 cm and the water level

(a) (b)

Figure 2: Scale foundation model. (a) Circular foundation. (b) Cone-shaped foundation.

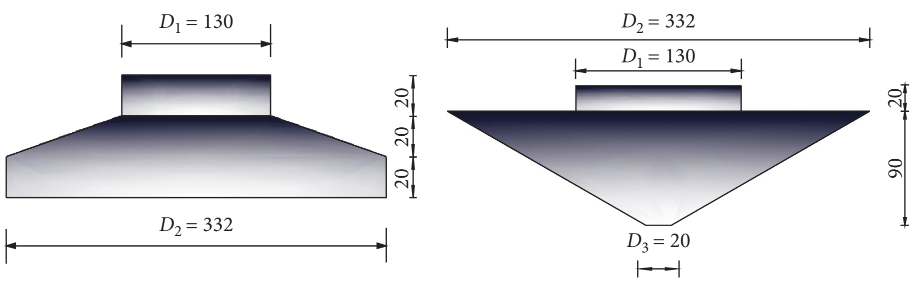

(a) (b)

Figure 3: Dimension of the scale foundation model. (a) Circular foundation. (b) Cone-shaped foundation. Unit: mm.

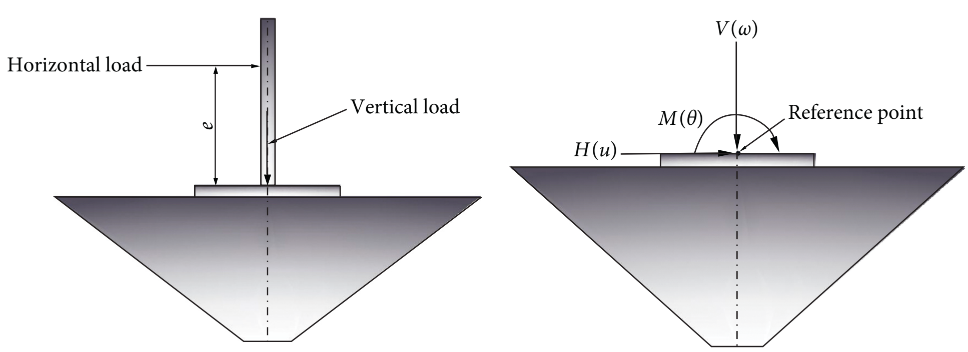

(a) (b)

Figure 4: Scale model for cone-shaped foundation. (a) Loading setup of the test. (b) Reference point and notation of displacements.

was higher than the sand surface, the dry marine fine sand was no longer sprayed into the tank.

2.6. Testing Procedures. In test, the relative density for the marine fine sand for all the tests should be in the same state so that the test results can be reproducible. Then, prior to the start of each test, the marine fine sands in the tank should be loosened to a depth of about 1.5 times the height of foundation so that the same stress level could be achieved [21]. The foundation model was buried into the loosened marine fine sands, then the water was poured into the tank, and the water level was kept to 3 cm high above the sand surface. Then the drain value was opened until no water flowed out of the drain valve. In the test, this process should be repeated twice. Before test starting, the foundation model should be placed in the sand for 6 hours. With this method, the relative density of the sand in the tank could reach a high value of 95.8%.

In this study, when the foundation model was subjected to constant vertical load (only considering the self-weight of the foundation model), the horizontal load (H) was applied to the loading rod embedded into foundation. Then the bending moment (M) can be calculated with the horizontal

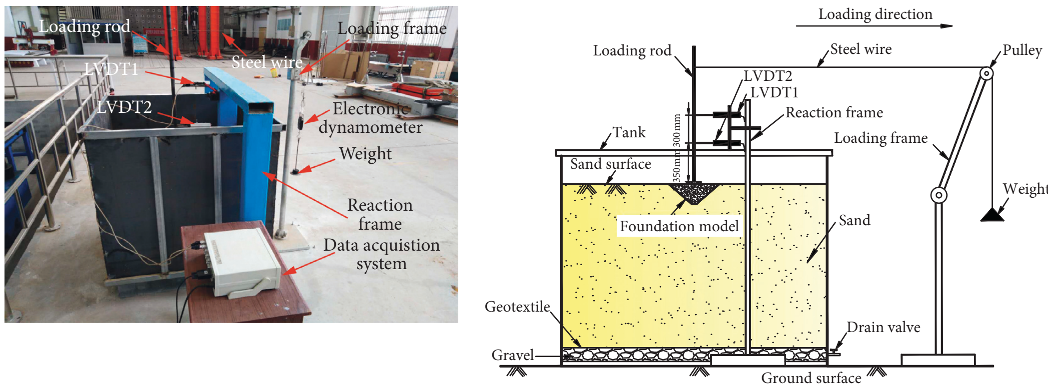

(a) (b)

Figure 5: Experiment setup. (a) Setup. (b) Schematic.

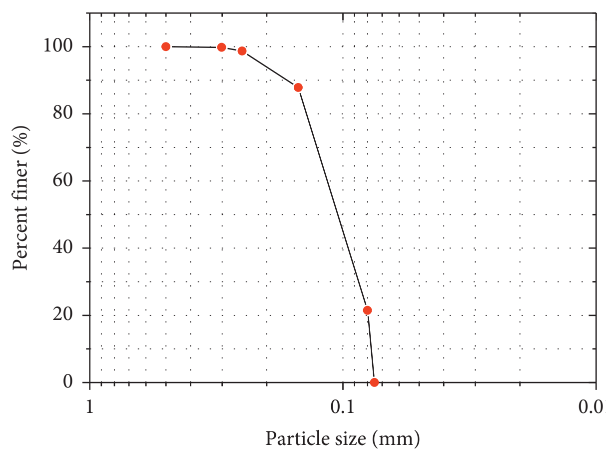

Figure 6: Particle size distribution curve.

Table 1: Physical parameters for sand used in the test.

e_{min}	e_{max}	e_0	D_{50} mm	ϕ (°)	C_u	C_c	K (cm/s)	γ_d (kN/m^3)	γ' (kN/m^3)	G_s
0.59	0.91	0.65	0.1008	38	1.8	0.994	0.0029	19.5	10.6	2.68

load (H) and the loading eccentricity (e), which acted on the top of foundation. In this paper, the loading eccentricity (e) was defined as M/HD_1, where D_1 was the diameter of the top of foundation (Figures 3(a) and 3(b)). Moreover, the load path can be also described with M/HD_1.

In the test, the horizontal load was applied to the loading rod by increasing the weight gradually, with an incremental horizontal load of 0.05 N for each step. In this paper, the normalised eccentricities $M/(HD_1)$ with regard to the top of foundation model were set to be 5.0, 6.0, and 7.0, respectively. In order to minimize errors, each load step should be sustained for at least 10 minutes until the deflection rate of the loading point was less than 0.015 mm after 10 minutes, and then the next load step began. The ultimate failure state represented the case where excessive displacements of the foundation model occurred without any increase in the applied horizontal load. The loading test procedure mentioned above should be repeated three times to ensure the maximum error for maximum horizontal load to be within 5%.

3. Test Results and Discussion

Kelly et al. [22] considered that, in most cases, the dimensionless small-scale laboratory test results for suction caissons subjected to moment loading can be scaled to the field. Therefore, the H-M bearing capacity of cone-shaped foundation model and conventional circular foundation model was investigated by carrying out the small-scale model tests in this study. Moreover, the results obtained from laboratory test can be used to verify the results of numerical analyses, which would be used to investigate the influence factors of the bearing capacity of cone-shaped foundation.

In this study, in consideration of strength in drained sand, the horizontal load applied to the loading rod was normalised as $H/[2\pi(D_1/2)^3\gamma']$, where D_1 was the diameter of top of the foundation model (Figures 3(a) and 3(b)) and γ' was the unit weight of the sand. In addition, the bending moment acting on the top of reference point of the foundation model was normalised as $M/[2\pi(D_1/2)^4\gamma']$, where D_1 was the diameter of top of the foundation model and γ' was the unit weight of the sand. Moreover, in this paper, $H_{\max}$ and $M_{\max}$ referred to the maximum horizontal load and moment of the foundation model under certain load path of M/HD_1. Besides, the horizontal displacement of the location where the horizontal loading was applied was normalised as L/D_1, where L was the deflection of the loading rod measured by LVDT1 in test.

3.1. Relationship between Horizontal Load and Deflection. During loading tests, the relationships between horizontal load and deflection of the loading rod for cone-shaped foundation under various loading eccentricities are shown in Figure 7. As can be seen from Figure 7, in all cases, the relationships between horizontal load and deflection of the loading rod can be well fitted with the quadratic function.

In Figure 7, all the horizontal displacement-horizontal load curves can be divided into three phases: Zone I (quasi-elastic), Zone II (plastic), and Zone III (failure phase). It can be observed from Figure 7 that the horizontal bearing capacity increased with decreasing loading eccentricity for circular foundation and cone-shaped foundation. In addition, at the same loading eccentricity, the horizontal bearing capacity for cone-shaped foundation was greater than circular foundation and the lateral deflection for cone-shaped foundation was lower than circular foundation, as can be seen from Figure 8. Besides, the ultimate bearing capacity for circular foundation and cone-shaped foundation can be derived from Figure 8 and is shown in Table 2. It can be observed from Table 2 that the resulting increment ratio of ultimate bearing capacity for cone-shaped foundation to circular foundation ranged from the minimum of 36.7% to the maximum of 53.9%.

In Zone I (quasi-elastic phase), the maximum horizontal displacement of the loading point was within 0.0062 D_1 for cone-shaped foundation and within 0.0071 D_1 for circular foundation in all cases, and the horizontal load increased nearly linearly with increasing horizontal displacement. In the quasi-elastic phase, the heave and settlement of sand around the foundation model was very small and not noticeable. In Zone II (plastic phase), the curves of horizontal load-deflection showed nonlinear relationships, mainly depending on loading eccentricity. In addition, the subsidence and upheaval of sand around the foundation model was more obvious than the quasi-elastic phase. In the plastic phase, the deflection increased greatly with the applied horizontal load, which reached peak value, H_{ult}.

In the failure phase, all the horizontal displacement-horizontal load curves showed great increase in the horizontal displacement with slowly increasing horizontal load, obviously showing the deflection-hardening behavior for the foundation model under different loading eccentricities.

In the plastic phase, based on the ultimate horizontal load H_{ult}, the ultimate moment M_{ult} can also be obtained, which was with respect to the loading eccentricity e. The relationship between ultimate horizontal load H_{ult} and ultimate moment M_{ult} for cone-shaped foundation and

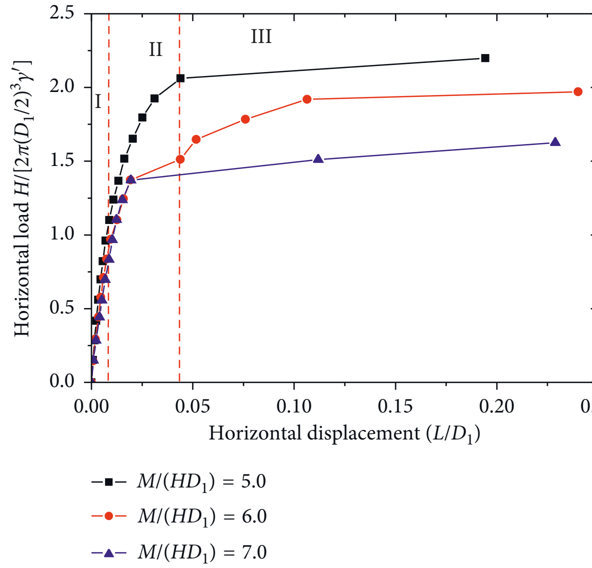

FIGURE 7: Horizontal displacement-horizontal load curves under different $M/(HD_1)$ values for cone-shaped foundation.

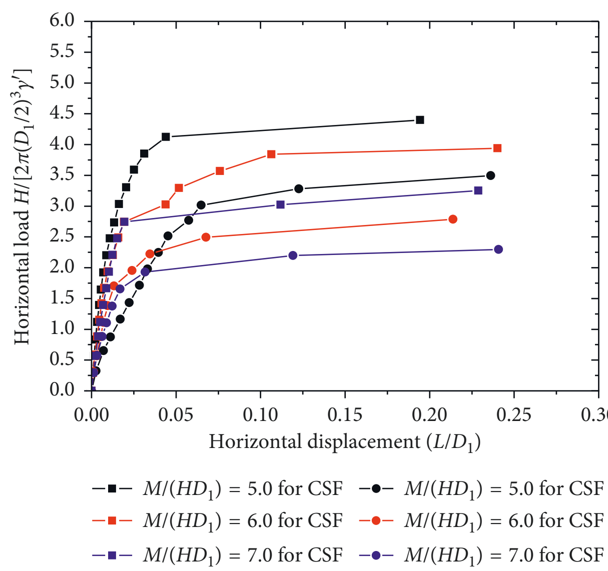

FIGURE 8: Comparison of horizontal displacement-horizontal load curves for cone-shaped foundation with circular foundation under different $M/(HD_1)$ values.

circular foundation in the load plane of H-M at various $M/(HD_1)$ ratios is shown in Figure 9. As can be seen from Figure 9, ultimate moment M_{ult} acting on the top and ultimate horizontal load H_{ult} of cone-shaped foundation were greater than circular foundation at same loading eccentricity, respectively. In addition, ultimate moment M_{ult} and ultimate horizontal load H_{ult} for the cone-shaped foundation model and circular foundation model increased with decreasing loading eccentricity, respectively.

In summary, the H-M bearing capacity for cone-shaped foundation decreased with increasing loading eccentricity. The deflection-hardening behavior of the horizontal displacement-

Table 2: Ultimate bearing capacity for the CSF model and CF model under various loading eccentricities.

Loading eccentricity (M/HD_1)	H_{ult} (CSF)	H_{ult} (CF)	Increment ratio of CSF to CF (%)
5.0	4.12445	3.01675	36.7
6.0	3.84000	2.49436	53.9
7.0	2.74325	1.93094	42.1

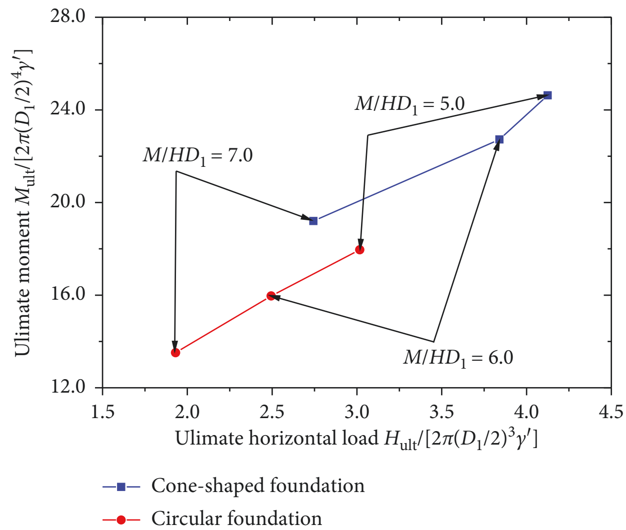

Figure 9: *H-M* interaction diagram.

horizontal load curves for cone-shaped foundation was very obvious under different loading eccentricities. In addition, the *H-M* bearing capacity for cone-shaped foundation was larger than circular foundation at the same loading eccentricity.

4. Ultimate Horizontal Bearing Capacity for Cone-Shaped Foundation

In this section, based on the limit equilibrium method, the ultimate horizontal bearing capacity for cone-shaped foundation was deduced, which was suitable for small deformation.

4.1. Computation Model. In this study, the computation model for the cone-shaped foundation embedded in the soil layer is shown in Figures 10(a) and 10(b). Figures 10(a) and 10(b) are the elevation and vertical views of the computation model, respectively.

When the computation model was in the limit equilibrium state, earth pressure and friction between cone-shaped foundation and soil, which were behind the ultimate horizontal force H_{ult} (Figure 10(a)), can be neglected. In addition, under the condition of small deformation assumed in the process of derivation, the computation model rotated around point o_1, as shown in Figure 10(a). Moreover, the soil layer in front of the ultimate horizontal force H_{ult} was assumed to be subjected to passive earth pressure, σ_p, which obeyed Coulomb's theory for passive earth pressure. Therefore, in the coordinate system shown in Figure 10, the passive earth pressure, σ_p, can be expressed as

$$\sigma_p = \gamma \cdot z \cdot K_p, \tag{1}$$

where H is height of cone-shaped foundation, z is the coordinate value along the z-axis, γ is the bulk weight of soil, and K_p is the coefficient of passive earth pressure, which is expressed as [23]

$$K_p = \frac{\cos^2(\varphi + (\pi/2) - \theta)}{\cos^2(\pi/2 - \theta)\cos((\pi/2) - \theta - \delta)\left[1 - \sqrt{(\sin(\varphi+\delta)\sin\varphi)/(\cos((\pi/2) - \theta - \delta)\cos((\pi/2) - \theta))}\,\right]}, \tag{2}$$

where φ is the angle of internal friction and δ is the frictional coefficient for soil and cone-shaped foundation.

As shown in Figure 10(b), in the plane of x-y, earth pressure on the surface of cone-shaped foundation can be expressed as

$$\sigma_r = \sigma_p \cdot \cos\beta, \quad 0 \le \beta \le \frac{\pi}{2}. \tag{3}$$

Therefore, based on σ_r, the component of earth pressure along the x-axis and the component of earth pressure along the y-axis in the plane of x-y can be further expressed as, respectively,

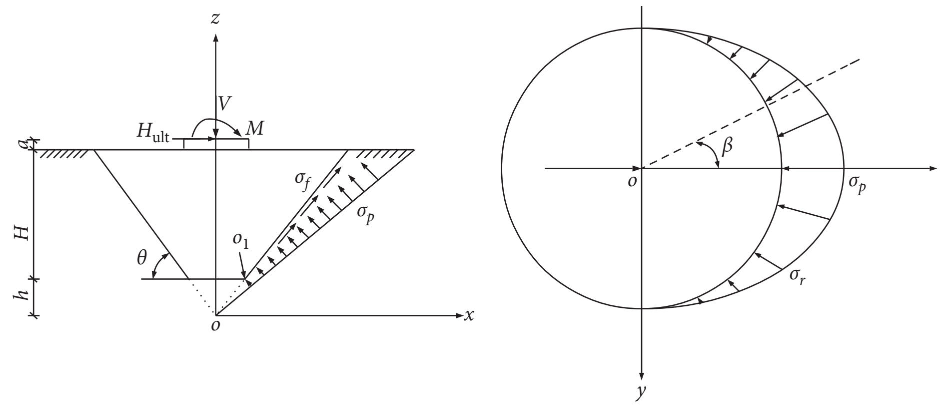

(a)

(b)

Figure 10: Distribution earth pressure along the surface of cone-shaped foundation.

$$\sigma_x = \sigma_r \cdot \cos\beta \cdot \sin\theta = \sigma_p \cdot (\cos\beta)^2 \cdot \sin\theta,$$
$$\sigma_y = \sigma_r \cdot \cos\beta \cdot \cos\theta = \sigma_p \cdot (\cos\beta)^2 \cdot \cos\theta, \quad (4)$$

and the friction stress on the surface of cone-shaped foundation can be expressed as

$$\sigma_f = \sigma_r \cdot \tan\delta = \sigma_p \cdot \cos\beta \cdot \tan\delta, \quad (5)$$

where δ is the interface friction angle produced by cone-shaped foundation and soil, which can be determined according to the test.

4.2. Ultimate Horizontal Force Based on Limit Equilibrium. In this section, the ultimate horizontal force H_{ult} can be deduced with static equilibrium based on the above-mentioned assumption.

Based on Figures 10(a) and 10(b), the resultant force of the passive earth pressure, parallel to the x-axis, can be expressed as

$$\begin{aligned} F_1 &= \int \sigma_p \cdot (\cos\beta)^2 \cdot \sin\theta \cdot \mathrm{d}A \\ &= 2\int_h^{H+h} \gamma \cdot K_p \cdot \cos\theta \cdot z^2 \cdot \mathrm{d}z \cdot \int_0^{\pi/2} (\cos\beta)^2 \cdot \mathrm{d}\beta \\ &= \frac{1}{12} \cdot \pi \cdot \gamma \cdot K_p \cdot \left(H^3 + 3H^2h + 3Hh^2\right) \cdot \cos\theta. \end{aligned} \quad (6)$$

Therefore, the moment produced by the resultant force of the passive earth pressure, P_1, at the point of $o_1$can be expressed as

$$\begin{aligned} M_{F_1} &= p_1 \cdot \left[\frac{H(2H+3h)}{3(H+2h)}\right] = \frac{1}{36} \cdot \pi \cdot \gamma \cdot K_p \\ &\quad \cdot \cos\theta \cdot \frac{H\left(H^3 + 3H^2h + 3Hh^2\right)(2H+3h)}{H+2h}. \end{aligned} \quad (7)$$

In addition, the resultant force of the passive earth pressure, parallel to the y-axis, can be expressed as

$$\begin{aligned} F_2 &= \int \sigma_p \cdot (\cos\beta)^2 \cdot \cos\theta \cdot \mathrm{d}A \\ &= 2\int_h^{H+h} \gamma \cdot K_p \cdot \sin\theta \cdot z^2 \cdot \mathrm{d}z \cdot \int_0^{\pi/2} (\cos\beta)^2 \cdot \mathrm{d}\beta \\ &= \frac{1}{12} \cdot \pi \cdot \gamma \cdot K_p \cdot \left(H^3 + 3H^2h + 3Hh^2\right) \cdot \sin\theta. \end{aligned} \quad (8)$$

Therefore, the moment produced by the resultant force of the passive earth pressure, P_2, at the point of $o_1$can be expressed as

$$\begin{aligned} M_{F_2} &= p_2 \cdot \left[\frac{H(2H+3h)}{3(H+2h)}\right] \tan\theta = \frac{1}{36} \cdot \pi \cdot \gamma \cdot K_p \\ &\quad \cdot \sin\theta \cdot \frac{H\left(H^3 + 3H^2h + 3Hh^2\right)(2H+3h)}{H+2h}. \end{aligned} \quad (9)$$

Based on Figures 10(a) and 10(b), the resultant force of the friction stress on the surface of cone-shaped foundation, parallel to the x-axis, can be expressed as

$$\begin{aligned} F_3 &= \int \sigma_p \cdot \cos\beta \cdot \tan\delta \cdot \cos\theta \cdot \mathrm{d}A \\ &= 2\int_h^{H+h} \gamma \cdot K_p \cdot \tan\delta \cdot \frac{\cos\theta^2}{\sin\theta} \cdot z^2 \cdot \mathrm{d}z \cdot \int_0^{\pi/2} \cos\beta \cdot \mathrm{d}\beta \\ &= \frac{2}{3} \cdot \gamma \cdot K_p \cdot \tan\delta \cdot \frac{\cos\theta^2}{\sin\theta}\left(H^3 + 3H^2h + 3Hh^2\right), \end{aligned} \quad (10)$$

and the resultant force of the friction stress on the surface of cone-shaped foundation, parallel to the y-axis, can be expressed as

$$F_4 = \int \sigma_p \cdot \cos\beta \cdot \tan\delta \cdot \sin\theta \cdot \mathrm{d}A$$
$$= 2\int_h^{H+h} \gamma \cdot K_p \cdot \tan\delta \cdot \cos\theta \cdot z^2 \cdot dz \cdot \int_0^{\pi/2} \cos\beta \cdot \mathrm{d}\beta$$
$$= \frac{2}{3} \cdot \gamma \cdot K_p \cdot \tan\delta \cdot \cos\theta\left(H^3 + 3H^2h + 3Hh^2\right). \tag{11}$$

When the cone-shaped foundation was in the limit equilibrium state, all vertical forces were in the equilibrium state, and the following equilibrium equation can be obtained, i.e.,

$$\begin{cases} \Sigma F_y = F_2 + F_4 - V = 0, \\ \Sigma M_{O1} = M_{F_1} + M_{F_2} - H_{ult} \cdot (H + e + a) + V \cdot \dfrac{h}{\tan\theta} = 0, \end{cases} \tag{12}$$

where e is the distance from the loading point for horizontal loading to the top of cone-shaped foundation and V is the vertical loading, including self-weight of cone-shaped foundation and wind turbine tower. Therefore, the ultimate horizontal bearing capacity for cone-shaped foundation, H_{ult}, can be expressed as

$$H_{\mathrm{ult}} = \gamma \cdot K_p\left(H^3 + 3H^2h + 3Hh^2\right) \cdot \frac{12 \cdot \pi \cdot H(2H + 3h)(\sin\theta \cdot \tan\theta + \sin\theta) + 36h(H + e + a)(H + 2h)(\pi\sin\theta + 8\tan\delta \cdot \cos\theta)}{432(H + e + a)(H + 2h) \cdot \tan\theta}. \tag{13}$$

4.3. Verification of Ultimate Horizontal Bearing Capacity. In this section, the validity of ultimate horizontal bearing capacity for cone-shaped foundation was verified according to comparing with the test results mentioned above. In test, the distance from the loading point for horizontal loading to the top of cone-shaped foundation, e, was 650 mm, 780 mm, and 910 mm, respectively, and other parameters were $a = 20$ mm, $\theta = 30^\circ$, $H = 90$ mm, $h = 17.32$ mm, $\varphi = 38^\circ$, $\gamma = 10.6\,\mathrm{kN/m^3}$, and $\delta = 26^\circ$, respectively. Therefore, the ultimate horizontal bearing capacity for cone-shaped foundation calculated based on equation (13) and obtained from test are shown in Table 3. As can be seen from Table 3, the maximum error was 18.2% and it showed that the ultimate horizontal bearing capacity for cone-shaped foundation calculated based on equation (13) fitted well with that obtained from the test.

5. Numerical Modeling

In this study, in order to explore the influence factors on bearing capacity for cone-shaped foundation, numerical analyses were carried out with Z_SOIL software [24]. Therefore, a three-dimensional numerical modeling was used to investigate the effect of the aspect ratio, embedded depth, and loading eccentricity on the bearing capacity for cone-shaped foundation. In addition, the numerical simulations used in this paper were only limited to *H-M* space.

5.1. Finite Element Model. In this research, boundary extension of the sand domain and the divided meshes for cone-shaped foundation and sand are represented in Figure 11. In the x, y, and z directions, displacements at the bottom boundary for the sand domain were fully fixed, and horizontal displacements at lateral boundaries were also constrained. In order to avoid boundary effects, the dimension of the sand domain should be sufficiently large enough. Bienen et al. [25, 26] considered that the soil domain with $7D$ in diameter and $6.25D$ in height, where D was the diameter of caisson foundation, could reduce boundary effects. However, Hung and Kim [27] considered that the soil domain with $9D$ in diameter and $5.5D$ in height could reduce boundary effects. Therefore, in this study, the dimension of the sand domain was $9D_2$ in diameter and $6.25D_2$ in height, where D_2 was the diameter of top of cone-shaped foundation in Figures 3(a) and 3(b). In addition, the notation of displacement and the reference point are shown in Figure 4(b).

5.2. Constitutive Model. In this research, the constitutive model of hardening small strain (*HSS*) was used to model the sand, which can simulate basic macroscopic behaviors exhibited by sand, such as stress-dependent stiffness, densification, dilatation, and soil stress history [28]. In addition, the constitutive model can obtain more reliable and accurate approximation of displacements. Compared with other constitutive models, the *HSS* constitutive model can better simulate the reduction of soil stiffness with shear strain amplitudes increasing. Moreover, as the *HSS* constitutive model accounted for prefailure nonlinearities, it was applicable to sand [29]. In the *HSS* constitutive model, eight-node continuum brick elements were used in cone-shaped foundation and sand. In addition, the cone-shaped foundation-sand interface was simulated using contact surface element in Z_Soil software, and the frictional angle between the cone-shaped foundation and the sand, φ_1, is shown in Table 4. In addition, the cone-shaped foundation had Young's modulus of 210 GPa and Poisson's ratio of 0.31, and the density of the cone-shaped foundation was $78\,\mathrm{kN/m^3}$.

In the numerical modeling, two main steps were included. Firstly, in order to determine the initial stress state in sand, a geostatic stress step should be carried out, which accounted for the effects of sand and the weight of cone-

Table 3: Comparison of ultimate horizontal bearing capacity.

Loading eccentricity, e (mm)	H_{ult} obtained from test (N)	H_{ult} calculated by equation (13) (N)	Deviation (%)
650	55.15	46.85	15.0
780	45.6	37.42	17.9
910	35.3	28.86	18.2

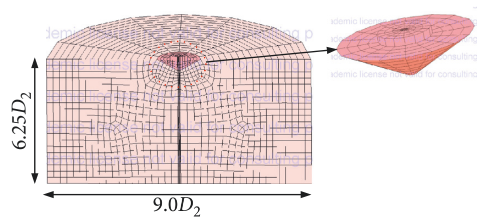

Figure 11: Finite element model.

Table 4: Parameters of sand used in the finite element model.

E_{ur} (kN/m^2)	N_{ur}	E_0^{ref} (kN/m^2)	$\gamma_{0.7}$	Ψ (°)	C (kPa)	E_{50}^{ref} (kN/m^2)	E_{oed} (kN/m^2)	K_0^{NC}	φ_1 (°)
12000	0.2	2600	0.000233	10	0	2505	800	0.41	26

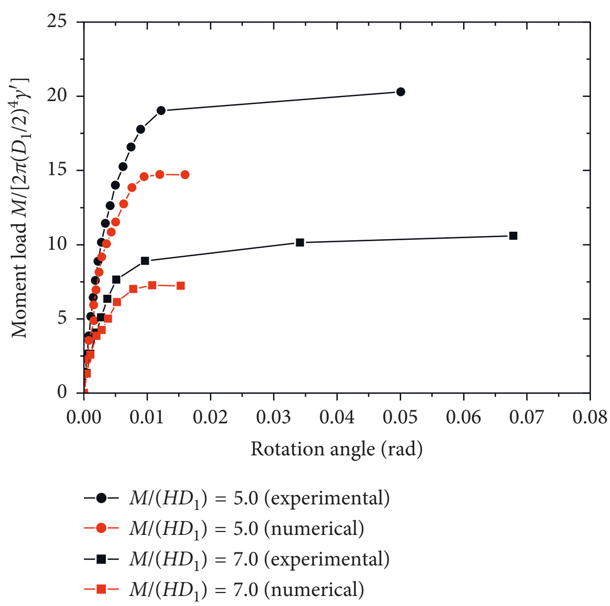

Figure 12: Comparison between test results and numerical results for moment against the rotation angle.

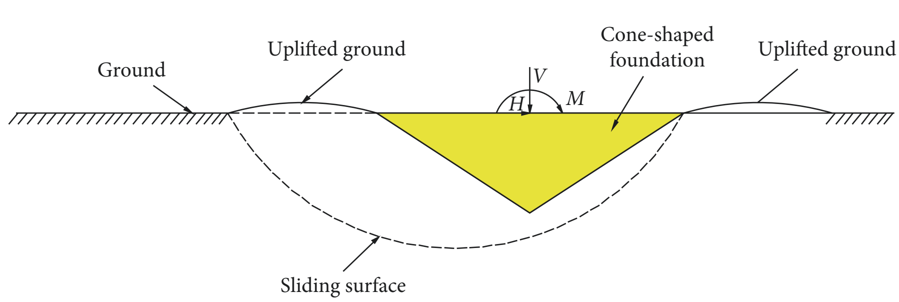

Figure 13: Failure mechanism for cone-shaped foundation.

shaped foundation. Then the second step was to impose the same monotonic horizontal load as the model test.

In the constitutive model of hardening small strain, the corresponding parameters for the sand are shown in Tables 1 and 4. In Table 4, the cohesion (c) and the internal friction angle (φ) were obtained by triaxial tests. Based on the finite element method, other parameters, such as E_{ur}, E_0^{ref}, and $\gamma_{0.7}$, were obtained according to back analysis. In order to verify the feasibility of the constitutive model of hardening small strain, a finite element model for scaled cone-shaped foundation shown in Figure 3(b) was built and the vertical loading applied to the reference point of scaled cone-shaped foundation was 0.014 kN. Figure 12 shows the comparisons of moment-rotation curves between numerical modeling and model tests. As can be seen from Figure 12, it was clear that sand parameters used in the constitutive model of hardening small strain by the back analysis were so reliable; therefore, the constitutive model of hardening small strain and the obtained bearing capacity were credible. Moreover, based on the method of finite element analyses, the failure mechanism for the cone-shaped foundation put forward by the authors is shown in Figure 13. As can be seen from Figure 13, general shear failure occurred when the cone-shaped foundation reached to limit state.

6. Results and Discussion

In this section, based on the numerical simulations, the factors influencing bearing capacity of cone-shaped foundation in the plane of H-M were investigated, such as aspect ratio, loading eccentricity, and embedded depth.

6.1. Effects of Aspect Ratio on Bearing Capacity. In the finite element model, the height of the cone-shaped foundation model was set to 3000 mm. In addition, the diameters D_3 and D_1 of the cone-shaped foundation model was set to 500 mm and 1000 mm, respectively, and the diameter D_2 varied between 2000, 4000, 6000, 8000, 10000, 12000, and 14000 mm, where D_2 and D_3 are shown in Figure 3(b). The nondimensional loading eccentricity M/HD_1 with respect to the top of the cone-shaped foundation model was 6.0. Besides, the vertical loading applied to the reference point of the cone-shaped foundation model was constant, which was 2000 kN.

As can be seen from the moment-rotation curves shown Figure 14(a), the bearing capacity increased with increasing aspect ratio. Moreover, when the aspect ratio was greater than 8/3, the relationship between moment and angular rotation showed more obvious linear elasticity. In addition, the rotation angles of the cone-shaped foundation at the same moment bearing capacity increased with decreasing aspect ratio. The variations of the maximum moment bearing capacity based on the aspect ratio are shown in Figure 14(b). Therefore, based on the maximum moment bearing capacity obtained by numerical analysis, equation (14) is expressed as the function of the ratio of the diameter D_2 of cone-shaped foundation to the height of cone-shaped foundation to estimate the maximum moment bearing capacity:

$$\frac{M_{max}}{2\pi (D_2/2)^4 \gamma'} = -0.21509 + 0.33298\left(\frac{D_2}{H}\right), \tag{14}$$

where M_{max} is the maximum moment bearing capacity and γ' is the natural gravity of sand used in the test.

6.2. Effects of Loading Eccentricity on Bearing Capacity. In order to investigate the effects of loading eccentricities on bearing capacity, the finite element model for cone-shaped foundation was the same as that described in Section 6.1. In addition, the diameter D_2 of the cone-shaped foundation model was set to 10000 mm. Moreover, the nondimensional loading eccentricities, M/HD_1, were set to 0, 1.5, 3.0, 4.5, 6.0, 7.5, and 9.0. The vertical loading applied to the reference point of the cone-shaped foundation model was also constant, which was 2000 kN.

Figure 15(a) shows the moment-rotation curves of the center of top of cone-shaped foundation under various loading eccentricities. As can be seen from Figure 15(a), the moment bearing capacity of the cone-shaped foundation increased with increasing loading eccentricity. Figure 15(b) shows the variations of the maximum moment bearing capacity with the loading eccentricity. The relationship between the maximum moment bearing capacity and the loading eccentricity was fitted by the binomial function, which can be expressed as

$$\frac{M_{max}}{2\pi (D_2/2)^4 \gamma'} = 2.19321 - 0.13138\left(\frac{M}{HD_2}\right) - 0.00803\left(\frac{M}{HD_2}\right)^2. \tag{15}$$

The H-M failure envelope of the cone-shaped foundation under various loading eccentricities at $V = 2000$ kN is shown in Figure 16(a), and the normalised H-M relationship is presented in Figure 16(b).

In order to illustrate the failure envelope of bucket foundation, in the load space of H-M-V, Murff [30] proposed an equation in terms of the horizontal load, moment load, and ultimate vertical load:

$$\left(\frac{V}{V_{ult}}\right)^2 + \left[\left(\frac{H}{H_{ult}}\right)^2 + \left(\frac{M}{M_{ult}}\right)^2\right]^{0.5} = 1. \tag{16}$$

In addition, in order to describe the coupled VHM bearing capacity of hybrid skirted foundation, Bienen et al. [25] proposed an equation:

$$\left(\frac{|H|}{H_{ult}}\right)^{1.4} + \left(\frac{|M|}{M_{ult}}\right)^{1.5} + \left(\frac{V}{V_{ult}}\right)^2 = 1. \tag{17}$$

As can be seen from Figure 16(b), the H-M relationship also satisfied the equations proposed by Murff and Bienen.

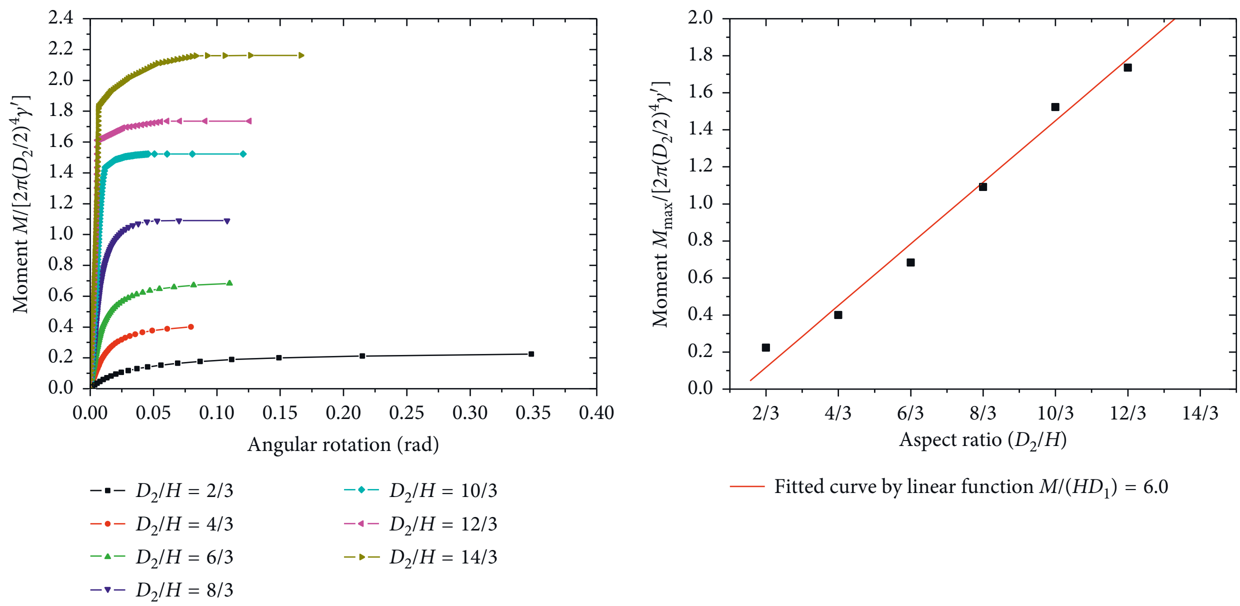

(a) (b)

FIGURE 14: Moment against the rotation angle under various aspect ratios. (a) Moment against rotation angle. (b) Maximum moment against aspect ratio.

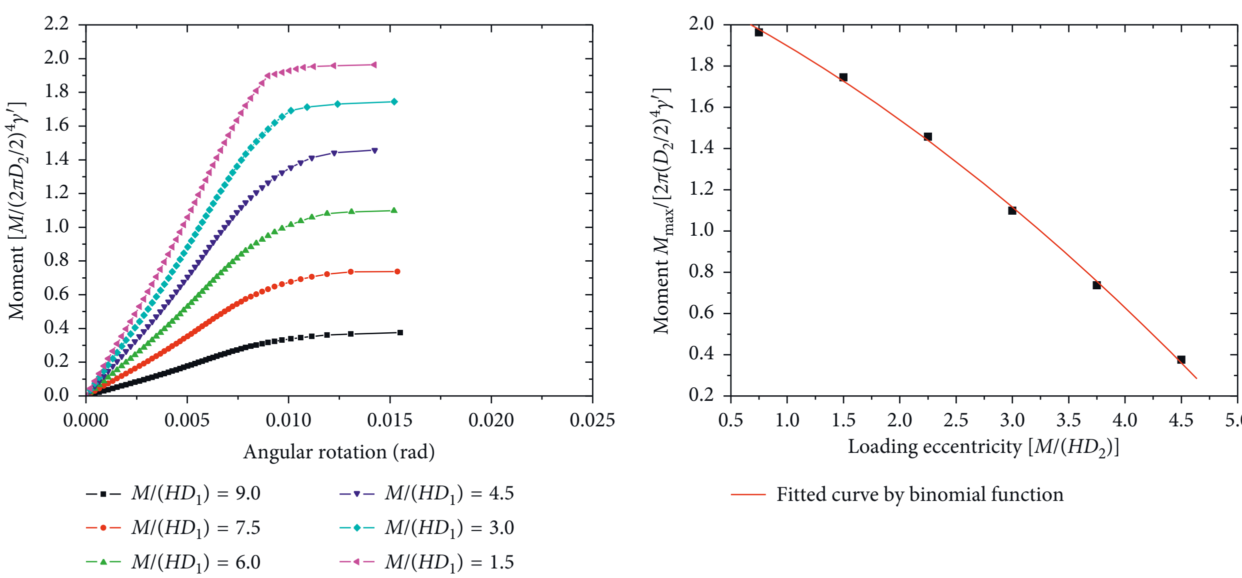

(a) (b)

FIGURE 15: Moment under various loading eccentricities. (a) Moment versus the rotation angle. (b) Maximum moment versus load eccentricity.

In this study, the fitted curve of the failure envelope of the cone-shaped foundation can be better expressed as

$$\left(\frac{|H|}{H_{\text{ult}}}\right)^{1.32}+\left(\frac{M}{M_{\text{ult}}}\right)^{1.45}+\left(\frac{V}{V_{\text{ult}}}\right)^{2}=1. \tag{18}$$

6.3. Effects of Embedded Depth on Bearing Capacity. To investigate the effects of embedded depth on bearing capacity, the height of the finite element model was set to 3000 mm. The embedded depth of cone-shaped foundation is shown in Figure 17. Besides, the diameters D_1, D_2, and D_3 of the cone-shaped foundation model are set to 1000 mm, 12000 mm, and 500 mm, respectively. The nondimensional loading eccentricity M/HD_1 with respect to the top of the cone-shaped foundation model was 6.0. In addition, the vertical loading applied to the reference point of the cone-shaped foundation model was constant, which was 2000 kN. Moreover, the embedded depth of cone-shaped foundation

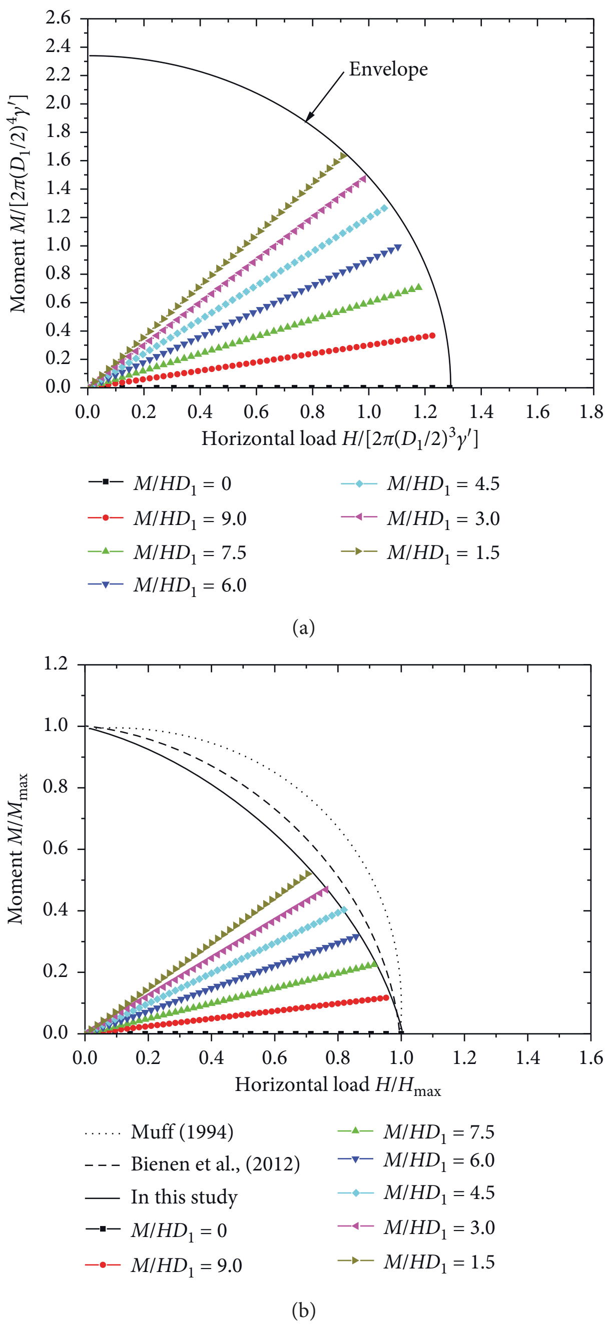

Figure 16: Failure envelope in H-M at $V = 2000$ kN for cone-shaped foundation. (a) H-M failure envelope. (b) Normalized form.

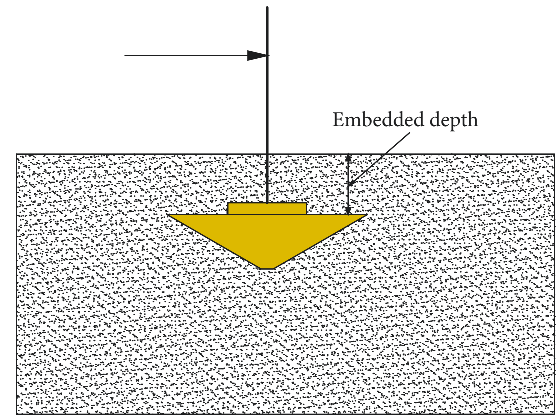

Figure 17: Schematic of embedded depth of the cone-shaped foundation model.

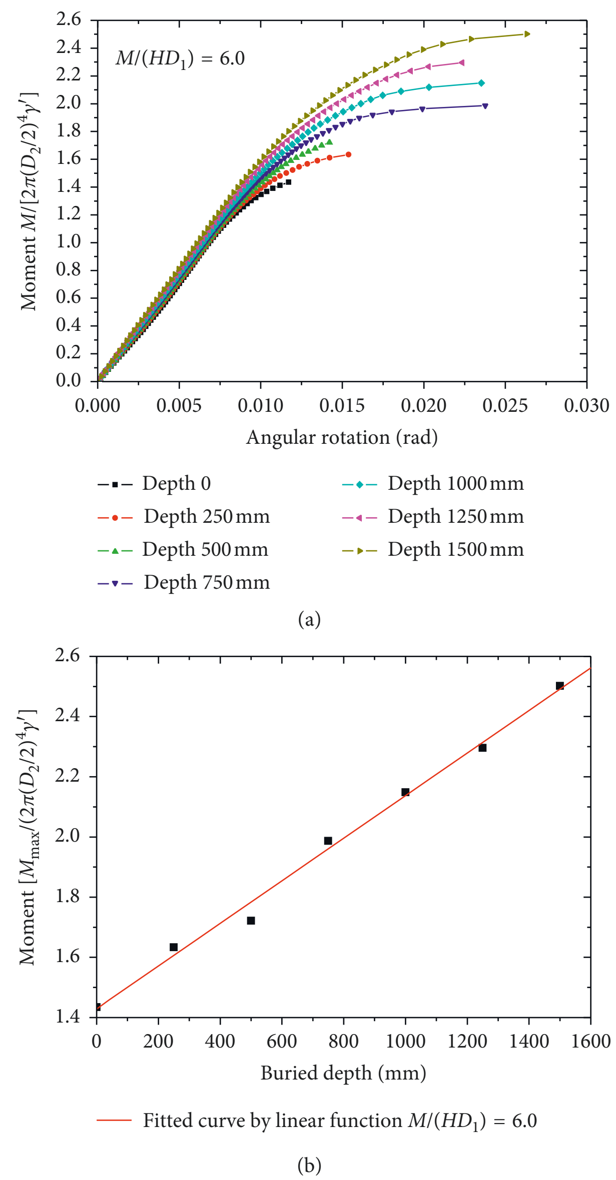

Figure 18: Moment versus rotation angle under various buried depths. (a) Moment versus rotation angle. (b) Maximum moment versus buried depth.

was set to 0, 250, 500, 750, 1000, 1250, and 1500 mm, respectively.

As can be seen from the load-deflection curves in Figure 18(a), the moment bearing capacity of the cone-shaped foundation increased with increasing embedded depth. The relationship between maximum moment bearing capacity and embedded depth is presented in Figure 18(b). By using the curve fitting technique, the binomial functional equation was proposed to estimate the maximum moment bearing capacity, taking the embedded depth into account:

$$\frac{M_{\max}}{2\pi (D_2/2)^4 \gamma'} = 1.42978 + 0.0007074h, \quad (19)$$

where h was the embedded depth of cone-shaped foundation.

7. Conclusion

In this study, a series of model tests were conducted on circular foundation and cone-shaped foundation in the marine fine sand under load-controlled horizontal combined loading to investigate the bearing behavior of cone-shaped foundation. In addition, a three-dimensional numerical analysis was also conducted to investigate the effects of aspect ratio, loading eccentricity $M/(HD_2)$, and embedded depth on the H-M bearing capacity of cone-shaped foundation in marine fine sand under monotonic horizontal loading. The following conclusions can be drawn:

(1) Compared with the circular foundation at the same loading eccentricity, the horizontal load and moment bearing capacity of cone-shaped foundation is larger and it increases with decreasing loading eccentricity under load-controlled methods.

(2) In dense sand, deflection-hardening behavior of the horizontal load-deflection curve for cone-shaped foundation is observed and becomes pronounced under different loading eccentricities.

(3) Finite element analysis results show that the aspect ratio, loading eccentricity, and buried depth had great influence on the horizontal and moment bearing capacity of cone-shaped foundation. In the limit state, the maximum moment bearing capacity increases with increasing aspect ratio based on the fitted curve by linear function between $M_{\max}/[2\pi(D_2/2)^4\gamma']$ and aspect ratio D_2/H. In addition, with increasing loading eccentricity, the maximum moment bearing capacity decreases. Moreover, maximum moment bearing capacity increases with increasing embedded depth of cone-shaped foundation.

(4) Expressions for maximum moment bearing capacity under different aspect ratios, loading eccentricities, and embedded depths had been proposed to describe the H-M bearing capacity of cone-shaped foundation in dense sand.

Data Availability

All the data used to support the findings of this study are included within the article.

Conflicts of Interest

The authors declare that there are no potential conflicts of interest with respect to the research, authorship, and/or publication of this article.

Acknowledgments

This research was financially supported by A Project of Shandong Province Higher Educational Science and Technology Program (Grant no. J17KB059), Doctoral Scientific Fund Project of Weifang University (Grant no. 2017BS14), and Science and Technology Project of High-Tech Zone in Weifang (Grant no. 2019KJHM09).

References

[1] Y. Wan, C. Q. Fan, Y. S. Dai et al., "Assessment of the joint development potentia of wave and wind energy in the south China Sea," *Energies*, vol. 11, no. 2, pp. 1–26, 2018.

[2] B. K. Sahu, "Wind energy developments and policies in China: a short review," *Renewable and Sustainable Energy Reviews*, vol. 81, no. 1, pp. 1393–1405, 2018.

[3] Y. Ling and X. Cai, "Exploitation and utilization of the wind power and its perspective in China," *Renewable and Sustainable Energy Reviews*, vol. 16, no. 4, pp. 2111–2117, 2012.

[4] G. Kariniotakis, D. Mayer, J. Moussafir et al., "Anemos: development of a next generation wind power forecasting system for the large-scale integration of onshore and offshore wind farms, EGS-AGU-EUG Joint Assembly," 2014, https://hal-mines-paristech.archives-ouvertes.fr/hal-00530475.

[5] A. Z. E. Wakile, "Horizontal capacity of skirted circular shallow footings on sand," *Alexandria Engineering Journal*, vol. 49, no. 4, pp. 379–385, 2010.

[6] L. Govoni, S. Gourvenec, and S. Gottardi, "Centrifuge modelling of circular shallow foundations on sand," *International Journal of Physical Modelling in Geotechnics*, vol. 10, no. 2, pp. 35–46, 2010.

[7] L. Govoni, S. Gourvenec, and G. Gottardi, "A centrifuge study on the effect of embedment on the drained response of shallow foundations under combined loading," *Géotechnique*, vol. 61, no. 12, pp. 1055–1068, 2011.

[8] L. B. Ibsen, A. Barari, and K. A. Larsen, "Modified vertical bearing capacity for circular foundations in sand using reduced friction angle," *Ocean Engineering*, vol. 47, pp. 1–6, 2012.

[9] A. A. Garakani and A. Ghaffar, "Numerical investigation on the bearing capacity of the spudcan foundation on sandy soils under applying static load," in *Proceedings of the Intemational Conference on Geotechnical Engineering and Soi Mechanics*, Tehran, Iran, November 2016.

[10] S. Shrestha and N. Ravichandran, "Design and analysis of foundations for onshore tall wind turbines," *Dessertations & Theses-Gradworks*, vol. 1, no. 1, pp. 217–226, 2015.

[11] A. Biswas and A. M. Krishna, "Behavior of circular footing resting on layered foundation: sand overlying clay of varying strengths," *International Journal of Geotechnical Engineering*, vol. 3, no. 3, pp. 114–116, 2017.

[12] W. Mohamed and P.-E. Austrell, "A comparative study of three onshore wind turbine foundation Solutions," *Computers and Geotechnics*, vol. 94, no. 1, pp. 46–57, 2018.

[13] G. G. Meyerhof, "Some recent research on the bearing capacity of foundations," *Canadian Geotechnical Journal*, vol. 1, no. 1, pp. 16–26, 1963.

[14] M. M. Liu, M. Yang, and H. J. Wang, "Study on subgrade reaction and punching of circular spread foundation for onshore wind turbines," *Acta Energiae Solaris Sinica*, vol. 36, no. 5, pp. 1130–1135, 2015.

[15] M. T. Luan, X. Y. Sun, X. W. Tang, and Q. L. Fan, "Lateral bearing capacity of multi-bucket foundation in soft ground," *China Ocean Engineering*, vol. 24, no. 2, pp. 333–342, 2010.

[16] Q. L. Fan and Y. F. Gao, "Effect of reinforcement ratio and vertical load level on lateral capacity of bridge pile

foundations," *Polish Maritime Research*, vol. 25, no. S3, pp. 120–126, 2018.
[17] J. Ching and K.-K. Phoon, "A quantile-based approach for calibrating reliability-based partial factors," *Structural Safety*, vol. 33, no. 4-5, pp. 275–285, 2011.
[18] D. Y. Li, H. B. Zhai, Y. K. Zhang et al., "Cone-shaped hollow flexible reinforced concrete foundation for mountain wind turbines and construction method," ZL201410654765, China Patent, 2015.
[19] X. Y. Xu, Z. Liu, and D. Zhang, "Study on ground mechanical characteristics of tower foundation of wind turbine with capacity more than one megawatt," *Water Power*, vol. 38, no. 12, pp. 74–76, 2012.
[20] B. Zhu, D.-Q. Kong, R.-P. Chen, L.-G. Kong, and Y.-M. Chen, "Installation and lateral loading tests of suction caissons in silt," *Canadian Geotechnical Journal*, vol. 48, no. 7, pp. 1070–1084, 2011.
[21] D. Li, Y. Zhang, L. Feng, and Y. Gao, "Capacity of modified suction caissons in marine sand under static horizontal loading," *Ocean Engineering*, vol. 102, pp. 1–16, 2015.
[22] R. B. Kelly, G. T. Houlsby, and B. W. Byrne, "A comparison of field and laboratory tests of caisson foundations in sand and clay," *Géotechnique*, vol. 56, no. 9, pp. 617–626, 2006.
[23] K. G. Zhang and S. Y. Liu, *Soil Mechanics*, Tsinghua University Press, Beijing, China, 2010.
[24] Zace Services Ltd, *Zsoil.Pc2011 Manual*, Elmepress International, Lausanne, Switzerland, 2011.
[25] B. Bienen, C. Gaudin, M. J. Cassidy, L. Rausch, O. A. Purwana, and H. Krisdani, "Numerical modelling of a hybrid skirted foundation under combined loading," *Computers and Geotechnics*, vol. 45, pp. 127–139, 2012.
[26] B. Bienen, C. Gaudin, M. J. Cassidy et al., "Numerical modeling of undrained capacity of hybrid skirted foundation under combined loading," *International Journal of Offshore and Polar Engineering*, vol. 22, no. 3, pp. 1–7, 2012.
[27] L. C. Hung and S. R. Kim, "Evaluation of vertical and horizontal bearing capacities of bucket foundations in clay," *Ocean Engineering*, vol. 52, pp. 75–82, 2012.
[28] C. R. I. Clayton, "Stiffness at small strain: research and practice," *Géotechnique*, vol. 61, no. 1, pp. 5–37, 2011.
[29] T. Benz, *Small-strain stiffness of soils and its numerical consequences*, Ph.D. thesis, Universitat Sttutgart, Stuttgart, Germany, 2007.
[30] J. D. Murff, "Limit analysis of multi-footing foundation systems," in *Proceedings of the 8th International Conference on Computer Methods and Advances in Geomechanics*, pp. 223–244, Morgantown, WV, USA, May 1994.


The Scientific World Journal
Journal of Applied Chemistry
Journal of Nanomaterials
Scientifica
International Journal of Polymer Science

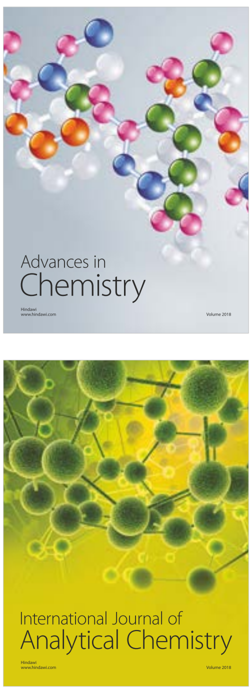
Advances in Chemistry
International Journal of Analytical Chemistry

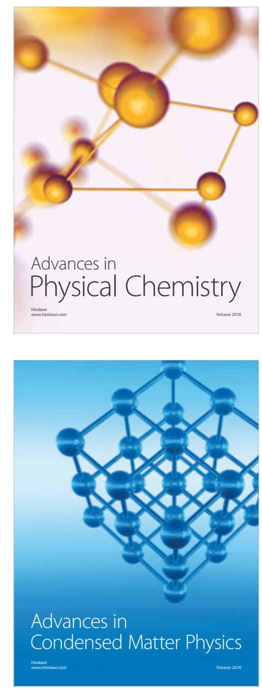
Advances in Physical Chemistry
Advances in Condensed Matter Physics


Journal of Chemistry
International Journal of Biomaterials
Advances in High Energy Physics
Journal of Engineering
Journal of Nanotechnology
International Journal of Corrosion
Journal of Materials
BioMed Research International
Advances in Tribology
Advances in Materials Science and Engineering